Original Article

Magnetic Resonance Gd-RGD Imaging Study of Hepatocellular Carcinoma with High and Low Metastatic Potential before and after Human Bone Marrow-derived Mesenchymal Stem Cell Intervention

Tian-Ran Li[1], Ming-Hui Yu[1], Xiao-Bin Huang[2], Zhi-Jie Yang[2], Guang-Ming Lu[3], Yan-Jun Li[3]

[1]Department of Radiology, The 1st Affiliated Hospital of Chinese PLA General Hospital, Beijing 100048, China
[2]Department of Radiology, Chinese PLA 95th Hospital, Putian, Fujian 351100, China
[3]Department of Radiology, Chinese PLA Nanjing General Hospital, Nanjing, Jiangsu 210000, China

Abstract

Background: Biotherapy based on human bone marrow-derived mesenchymal stem cells (BMSCs) is currently the focus of research, especially in the field of autologous stem cell transplantation. A novel type of metastasis-associated magnetic resonance (MR) molecular imaging probe was constructed, and the changes in metastasis and proliferation of hepatocellular carcinoma (HCC) before and after BMSC intervention were observed through MR imaging (MRI).

Methods: Metastasis-associated MR molecular imaging probe, integrin $\alpha_v\beta_3$ ligand cRGD-PEG-DGL-DTPA-Gd (Gd-RGD), were constructed. After human BMSC intervention was performed for 6 weeks, tumor weight inhibition rates were calculated, and the RGD molecular probe was imaged through MRI with molecular imaging agent Gd-DTPA as control. The signal-to-noise ratio (SNR) and contrast-to-noise ratio (CNR) in the MRI experiment were used as semi-quantitative indicators. Polymerase chain reaction method was performed to detect proliferation- and metastasis-associated indicators, transforming growth factor β-1 (TGFβ1), osteopontin (OPN), and integrin subunit α_v and β_3.

Results: The highest tumor weight inhibition rates were observed 3 weeks after the BMSC transplantation. The MR Gd-RGD in the HCC tissues after the BMSC intervention showed less enhancement than Gd-DTPA. The Gd-DTPA MRI of control group had higher SNR and CNR than Gd-RGD MRI in the experimental groups ($P < 0.05$). For high metastatic potential hepatocellular carcinoma (MHCC97-H), significant differences were observed in the SNRs and CNRs of Gd-RGD MRI before and after the BMSC intervention ($P < 0.05$). For low metastatic potential hepatocellular carcinoma (MHCC97-L), the CNRs of Gd-RGD MRI were statistically different before and after BMSC intervention ($P < 0.05$). With regard to MHCC97-H, OPN, β_3, and TGFβ1 expression significantly decreased after BMSC intervention ($P < 0.05$). In MHCC97-L and OPN, β_3, TGFβ1, and α_v expression after BMSC intervention decreased, and the difference was statistically significant ($P < 0.05$).

Conclusions: The CNR index of MRI is a good indicator for distinguishing high- and low-metastatic potential HCC tissues. After BMSC transplantation of MRI through the two kinds of tracer, the SNR and CNR indexes can distinguish two kinds of high and low metastatic potential HCC tissues, and Gd-RGD imaging is more suitable in distinguishing the metastatic potential changes through BMSC intervention.

Key words: Arginine-Glycine-Aspartic Acid; Bone Marrow-derived Mesenchymal Stem Cells; High Metastatic Potential Hepatocellular Carcinoma; Integrin; Low Metastatic Potential Hepatocellular Carcinoma

Introduction

Biotherapy based on human bone marrow-derived mesenchymal stem cells (BMSCs) is currently the focus of research, especially in the field of autologous stem cell transplantation, which has potential applications in the treatment of multiple diseases, including hepatocellular carcinoma (HCC).[1,2] However, the possible long-term effects

Access this article online

Quick Response Code:

Website: www.cmj.org

DOI: 10.4103/0366-6999.217089

Address for correspondence: Prof. Tian-Ran Li, Department of Radiology, The 1st Affiliated Hospital of Chinese PLA General Hospital, Beijing 100048, China
E-Mail: lizhaoruixin@sina.com

Received: 19-06-2017 **Edited by:** Li-Min Chen
How to cite this article: Li TR, Yu MH, Huang XB, Yang ZJ, Lu GM, Li YJ. Magnetic Resonance Gd-RGD Imaging Study of Hepatocellular Carcinoma with High and Low Metastatic Potential before and after Human Bone Marrow-derived Mesenchymal Stem Cell Intervention. Chin Med J 2017;130:2591-600.

of using stem cells on tumors and the safety of this approach require further research. Our research group has focused on studying primary HCC including BMSCs on liver cancer before and after intervention of liver cancer tissue proliferation and metastatic behavioral changes.[3,4] The new HCC cell lines with high and low metastatic potential were constructed by the Liver Cancer Research Institute of Fudan University.[5] This cell line is the best model in studying the metastatic behavior of HCC.[6] In the paper, we adopted the HCC with high and low metastatic potential as the study object. In addition, the effectiveness of BMSC transplantation for tumor intervention can be observed in real time because of the progress in modern molecular imaging.[7,8] Molecular imaging probes, owing to their molecular structures, can bind to specific targets within living cells and thus facilitate the detection of the structures and properties of the targets and generation of signals that can be monitored in real time *in situ* and *in vivo*.[9] However, real-time monitoring of biological behaviors of the tumor *in vivo*, such as tumor proliferation and metastatic behaviors, before and after BMSC intervention, remains difficult. Integrin, an allotropic cell adhesion molecule, mediates the interaction between a cell and extracellular matrix (ECM), thereby facilitating tumor metastasis. Among known integrins, integrin $\alpha_v\beta3$ is the most important because it is abundant in superficial cells and neovascular endothelial cells of multiple tumors and participates in tumor angiogenesis.[10,11] An integrin $\alpha_v\beta_3$ receptor exerts its effect by specifically binding to the recognition sequence, arginine-glycine-aspartic acid (Arg-Gly-Asp, RGD), together with ECM protein.[12] This research aims to establish a novel type of metastasis-associated magnetic resonance (MR) molecular imaging probe, Gd-RGD, and observe the changes in HCC metastasis and proliferation behaviors before and after BMSC intervention through MR imaging (MRI).

Methods

Ethical approval

The animal study was approved by the Institutional Animal Care and Use Committee of the Chinese PLA General Hospital, China. Animal disposition during the experimental process conformed to the standard of medical ethics.

Establishment of molecular imaging probe and analysis of cRGD-PEG-DGL-DTPA-Gd

The established method of preparing an MRI molecular probe of RGD ligand for metastasis-associated factor integrin $\alpha_v\beta_3$ is as follows: first, DGL-PEG was synthesized. DGL (123 amino groups on surface, molecular weight 22,000 Da, 3 passages, COLCOM, France) was dissolved in methanol to form a working solution, which was then placed under sealed preservation at 4°C and the NHS group on PEG was specifically reacted with the primary amine on the DGL surface, generating DGL-PEG. Second, DGL-PEG-cRGD was synthesized. The N-terminal of cRGD peptide was connected to a cysteine to form a polypeptide containing free sulfhydryl groups. cRGD and DGL-PEG peptides were mixed to obtain a cRGD:DGL-PEG molar ratio of 10:1. The resulting solution was stirred under room temperature for 24 h to produce DGL-PEG-cRGD. Third, cRGD-PEG-DGL-DTPA was synthesized. DGL-PEG-cRGD and p-SCN-Bn-DTPA at 1:90 ratio were weighed and combined under room temperature in 50 ml of PBS with pH of 9.0 for 48 h. The molecular weight cutoff was 5000 Da for 24 h and dried to obtain a white solid powder. Finally, cRGD-PEG-DGL-DTPA-Gd was synthesized. The DGL-DTPA was re-dissolved in 2 ml 0.1 mol/L sodium acetate buffer pH 6.0, and excess gadolinium chloride hexahydrate was added. The reaction mixture was subjected to a temperature of 4°C for 24 h to obtain DGL-DTPA-Gd, and the product was freeze-dried and collected in pure water after purification by an ultrafiltration device.

The freeze-dried powder samples of the fresh compounds prepared above were dissolved in 0.5 ml of DMSO for nuclear magnetic resonance (NMR) analysis under a field strength of 600 MHz. The product samples were also dissolved in pure water after NMR analysis to determine GD content and calculate ligation efficiency through inductively coupled plasma-atomic emission spectrometry.

Calculation method of dosage of molecular probe

Experimental group

In the configuration method marked with 33.5 mg, 23.5 mg of drug and 15 ml of normal saline were used, while in that marked with 32.3 mg, 26.3 mg drug and 15 ml of normal saline were used. Both groups were separately packaged for subsequent use.

Control group

Magnevist solution (Gd-DTPA) was clinically used at 20 ml from the dilution of 9.38 g for 1000 times. Only 40 ml of aliquot was collected after dilution and separately packaged for standby use.

Final use concentration of animal models

Gd-DTPA and Gd-RGD concentrations were 1/10 and 1/1000 of the clinical concentration, respectively, while all contrast agent dosages were 0.4 ml. Scanning was implemented after 30 min delay.

Gd-RGD magnetic resonance imaging parameters and magnetic resonance imaging analysis method

MR GE Discovery HD750 (3.0 T), MR 3.0 T phased array radio frequency coils in mice from Shanghai ChenGuang Medical Technology Co., Ltd.; coil model: CG—MUC40-H300-AG (Bore Diameter: 5 cm). Scanning sequence was as follows: T2WI, T1WI, and T1WI + CE. Inspection equipment and scanning parameters were as follows: GE HD750 MR, Coil: HD 8Ch High Res Brain Array by *in vivo*, FOV 6.0 cm, slice thickness 3.0, slice spacing 0.5, NEX 1, pulse sequence: gradient echo, BEAVO, FSE-XL, SPGR, TR = 4600 ms, TE = 108.7 ms, layer thickness = 3.0, interlayer spacing = 1.0, matrix = 448 × 256, and FOV = 18 cm × l3.5 cm.

SNR and contrast-to-noise ratio (CNR) were used as semi-quantitative indexes.

SNR = SI tissue/standard deviation (SD) background

CNR = (SI lesion − SI tissue)/SD background.

Where SI tissue was a mean value of signal strength in one region of the liver tissue, and SD background was the SD of the blank background signal. Region of interests (ROIs) were drawn on the tumor, liver, and background region, and all ROI sizes had similar value in the triplicate measurements.

Preparation of hepatocellular carcinoma animal models

A total of 60 6-week-old healthy Balb/c SPF-level nude mice (30 males and 30 females) with weights ranging from 14 g to 17 g were provided by the Experimental Animal Center in China Biological Products Assay Institute. The experimental animal quality certification number was SCXK (J) 2009-0017, while the animal quality certification number was 0205939. The weight of each mouse was about 20 g during purchase. Drinking water was sterilized Grade-2 ultrapure water, and the quality of drinking water conformed to the PRC national standard, *Sanitary Standard for Domestic Drinking Water* (GB5749-2006). The usage license number of the experimental animal room was SYXK (Z) 2015-0008, and the feeding environment was as follows: nude mice were fed in an isolation cage supplemented by clean laminar-flowing cabinet in an animal feeding room with IVC-II (intelligent type) independent air supply. The temperature range was 20–25°C, and the range of relative humidity was 40–70%. The mice ate sterilized nude mice fodder at SPF level, which were products from the experimental animal research institution in CAMS. Human high and low metastatic potential HCCs (MHCC97-H and MHCC97-L) tumorous nodes, which were cultured *in vivo* through subcutaneous vaccination in mice bodies with favorable growth, were prepared into oncocyte patches through sterile operation and inoculated in the subcutaneous armpits of the mice with puncture needles. The nude mice were randomly divided into two groups with thirty in each group. One group was inoculated with MHCC97-H cells, while the other with MHCC97-L cells. The animals were weighted and labeled. Each group was randomly subdivided into the control group and experimental group again with 15 nude mice in each subgroup [Figure 1].

Bone marrow-derived mesenchymal stem cell intervention method

Tail intravenous injection of BMSCs (5×10^5/each mouse) was introduced 15 days after tumor inoculation in the experimental group. Tail intravenous injection of BMSC culture fluid was introduced to the mice in the control group (0.2 ml/each mouse). During the experiment, subcutaneous tumor volume was measured with a caliper each week, and three mice in each group were executed after 14, 21, 28, 35, and 42 days [Figure 2]. Tumor blocks were completely dissected out from the dead mice in each group. The weights of the tumor and mouse were measured, and the tumor weight inhibition rates were calculated. The detection indexes of tumor change before and after BMSC intervention of HCC tissues were calculated as follows:

Tumor weight inhibition rate (%) =

$$\left(1-\frac{\text{Average tumor weight in treatment group (T)}}{\text{Average tumor weight in control group (C)}}\right)\times 100\%$$

By week 6, only three animal models were left in each group. These animal models were used in MRI experiments before sacrificing.

Magnetic resonance imaging experiment grouping

Combining BMSC intervention experiment, we used stratified cross grouping. Molecular probe group: clinically used Gd-DTPA was the control group, while Gd-RGD served as the experimental group. Tumor model groups: blank tumor model was the control group and BMSCs were the experimental group. Each group of three tumor-bearing animal models was subjected to MRI. Every animal model used two probes at 12 h intervals for the MRI experiment.

Polymerase chain reaction detection

Primer sequence design: primer sequences of transforming growth factor β-1 (TGFβ1), osteopontin (OPN), and integrin subunits α_v and β_3 were provided from the GenBank database and synthesized by Cyagen (Guangzhou) Biotechnology Company [Table 1].

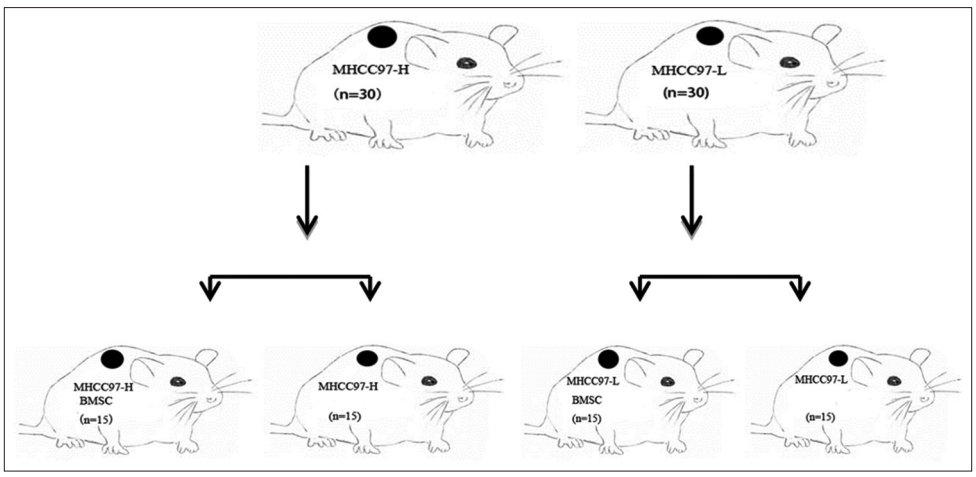

Figure 1: Animal model experimental grouping.

Experimental method

After the MHCC97-H cells adhered to the walls in the lower chamber, BMSCs were inoculated (3×10^4 cell counts per pore) in the upper chamber of the 12-pore plate. After co-culturing for 48 h, the cells in the lower chamber were sent for polymerase chain reaction (PCR) detection. The following methods were then performed: RNA extraction and application, RevertAid™ M-MLV RT reaction system and Oligo (dT) synthesis of cDNA, and amplification of the corresponding cDNA through PCR. The PCR conditions were as follows: premodification under 95°C for 5 min, 30 cycles that consisted of modification under 94°C for 30 s, annealing under 58°C for 30 s, and extension under 72°C for 30 s, and a final condition of 72°C for 10 min. PCR products were separated under electrophoresis and scanned through gel electrophoresis processing system for semi-quantitative analysis.

Statistical analysis

Experimental data were expressed as mean ± standard deviation (SD), and mean analysis in GraphPad Prism statistical software (GraphPad Software, San Diego, CA, USA) was used in the statistical test. The homogeneity of variance of the data was initially implemented when the variance was homogeneous. One-way variance analysis (ANOVA) was used to compare populations, and the comparison between two means in multiple dosage groups and one control group was used for statistics. Rank-sum test was used for the statistics of nonnormal data or data with heterogeneity of variance, and $\alpha = 0.05$ was used as test criterion.

Results

Gd-RGD magnetic resonance imaging result analysis of high metastatic potential hepatocellular carcinoma tumor before and after bone marrow-derived mesenchymal stem cell intervention

Gd-RGD and Gd-DTPA were used for the experimental and control groups, respectively. T1-weight image (TIWI) imaging sequences were used for MRI enhancement. TIWI MRI scanning was initially implemented before

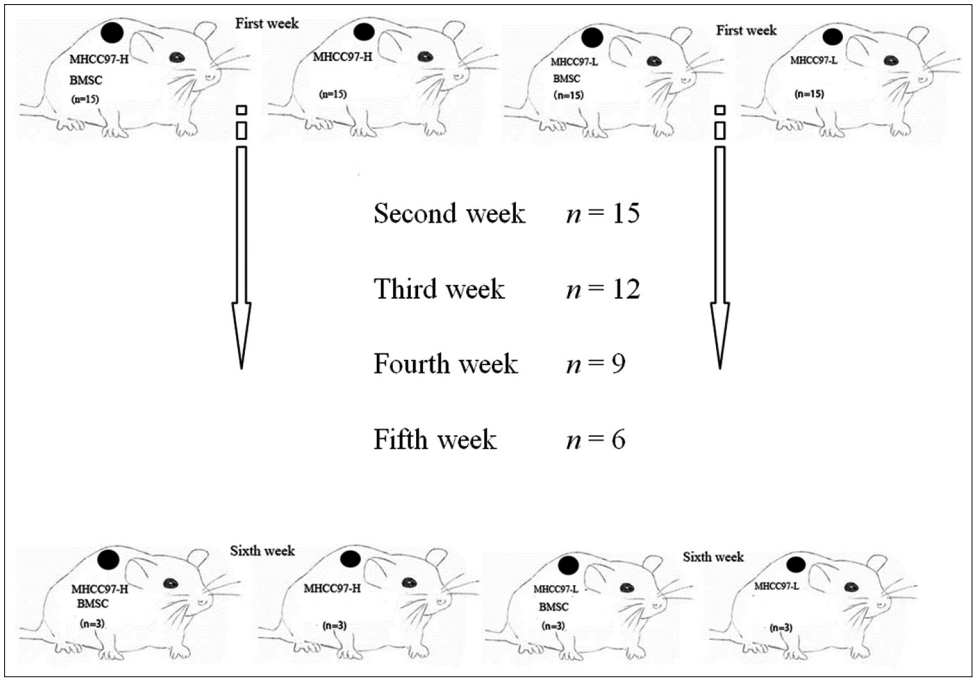

Figure 2: BMSC intervene experimental grouping. BMSC: Bone marrow-derived mesenchymal stem cell.

Table 1: List of primer sequences used for RT-PCR amplification of OPN, α_v, β_3, and TGFβ1

Primer name	Primer sequence	Product fragment length (bp)
OPN	Upstream: 5' GCAGAAGGAGATCACAGCCCT 3' Downstream: 5' GCTGATCCACATCTGCTGGAA 3'	331
α_v	Upstream: 5' CCTCAGACGCTGCGTGGAGC 3' Downstream: 5' AGGGCTGAGCTTCGGAGCGA 3'	314
β_3	Upstream: 5'-GTGCT-GACGCTAACTGACC-3' Downstream: 5'-CATGGTAGTGGAGGCAGAGT-3'	285
TGFβ1	Upstream: 5' AGTGGTTGAGCCGTGGAG 3' Downstream: 5' TGCAGTGTGTTATCCCTGCT 3'	155

RT-PCR: Reverse transcription-polymerase chain reaction; OPN: Osteopontin; TGFβ1: Transforming growth factor β-1.

conducting CE-TIWI imaging [Figures 3 and 4], and SNR and CNR were calculated as semi-quantitative indexes [Figures 5 and 6].

Tumor tissues were subjected to Gd-DTPA or Gd-RGD imaging. The Gd-RGD in HCC tissues before and after BMSC intervention was less enhanced than Gd-DTPA. Similarly, Gd-RGD in liver tissues was also less enhanced than Gd-DTPA in the absence of BMSC intervention.

SNR and CNR were calculated as quantitative indexes, and the results indicated that both SNR and CNR under Gd-DTPA imaging in the control group before and after BMSC intervention were higher than those under Gd-RGD imaging in the experimental group ($P < 0.05$).

Gd-RGD magnetic resonance imaging result analysis of low metastatic potential hepatocellular carcinoma tumor model before and after bone marrow-derived mesenchymal stem cell intervention

Gd-RGD and Gd-DTPA were used for the experimental group and the control group, respectively. MHCC97-L cells were inoculated at nude mouse armpits, and TIWI imaging sequences were used for MRI enhancement. TIWI MR scanning was initially implemented before conducting CE-TIWI imaging [Figures 7 and 8], and SNR and CNR were calculated [Figures 9 and 10].

MHCC97-L tumor tissues were observed in the armpits of mice and placed under Gd-DTPA and Gd-RGD imaging. Gd-RGD was less enhanced than Gd-DTPA both before and after the BMSC intervention on HCC tissues. Similarly, the Gd-RGD in liver tissues was also less enhanced than Gd-DTPA.

SNR and CNR were calculated as quantitative indexes, and the results showed that both SNR and CNR under Gd-DTPA imaging in the control group before and after BSMCs intervention were higher than those under Gd-RGD imaging in the experimental group ($P < 0.05$).

Comparative analysis of magnetic resonance imaging images before and after bone marrow-derived mesenchymal stem cell intervention of hepatocellular carcinoma tissues

SNR and CNR were adopted as semi-quantitative indexes to analyze the tumor imaging effects of the two tracers before and after BMSC intervention [Table 2].

After BMSC intervention for 6 weeks, Gd-RGD and Gd-DTPA imaging were implemented. SNR analysis showed no statistical difference between the SNRs of MHCC97-H and MHCC97-L through Gd-RGD imaging ($P > 0.05$). By contrast, SNR difference between MHCC97-H and MHCC97-L groups after BMSC intervention showed statistical significance ($P < 0.05$). The SNR results of Gd-DTPA imaging were identical to those of Gd-RGD imaging. CNR analysis of Gd-RGD imaging showed that the MHCC97-L group had significantly higher CNR indexes than the MHCC97-H group ($P < 0.05$). The CNR results of BMSC + MHCC97-L and BMSC + MHCC97-H groups were also significantly different ($P < 0.05$) after BMSC intervention. CNR

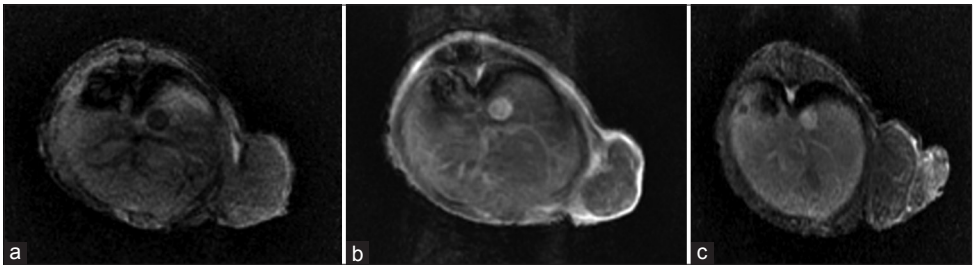

Figure 3: MRI of MHCC97-H tumor-bearing nude mice. (a) MRI scanning TI-weighted image. MHCC97-H tumor tissues were located at the mouse armpits. (b) Gd-DTPA-enhanced image. Enhanced pattern of the tumor tissue similar to that of the liver tissue. (c) Gd-RGD-enhanced image. Enhanced pattern of the tumor tissue is lower than that of the liver tissue. MRI: Magnetic resonance imaging; MHCC97-H: High-metastatic-potential hepatocellular carcinoma.

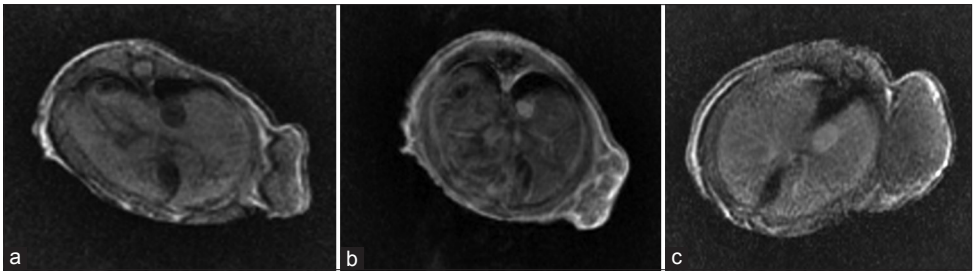

Figure 4: MRI of MHCC97-H tumor-bearing nude mice under BMSC intervention. (a) MRI scanning TI-weight image. MHCC97-H tumor tissues were located at the mouse armpits. (b) Gd-DTPA-enhanced image. Enhanced pattern of the tumor tissue is similar to that of liver tissue. (c) Gd-RGD-enhanced image. Enhanced pattern of the tumor tissue is lower than that of liver tissue. MRI: Magnetic resonance imaging; MHCC97-H: High-metastatic-potential hepatocellular carcinoma; BMSC: Bone marrow-derived mesenchymal stem cell.

results of Gd-DTPA imaging were identical with those of Gd-RGD imaging.

Comparison of both SNRs under Gd-RGD imaging before and after BMSC intervention of MHCC97-H showed statistical difference ($P < 0.05$), whereas comparison of SNR under Gd-DTPA imaging before and after BMSC intervention showed no statistical difference ($P > 0.05$) despite the statistical difference in CNR ($P < 0.05$).

The SNR under Gd-RGD imaging of MHCC97-L before the BMSC intervention was not statistically different from that after the intervention ($P > 0.05$) despite the statistical difference in CNR ($P < 0.05$). Comparison of both SNR and CNR under Gd-DTPA imaging before and after BMSC intervention showed no statistical difference ($P > 0.05$).

Changes of tumor weights before and after bone marrow-derived mesenchymal stem cell intervention

Tumor weights of MHCC97-H and MHCC97-L were observed beginning from the 2nd week after BMSC intervention.

After BMSC intervention, the weights of the tumor tissues decreased, indicating the inhibitory effect of BMSCs on the proliferation of tumor tissues. The tumor weight inhibition rates of MHCC97-H were 22.71%, 42.86%, 34.48%, 31.60%, and 29.17% on the 2nd, 3rd, 4th, 5th, and 6th weeks, respectively. Meanwhile, the tumor weight inhibition rates of MHCC97-L were 26.62%, 52.00%, 38.20%, 31.98%, and 30.23%, on the 2nd, 3rd, 4th, 5th, and 6th weeks, respectively. The tumor inhibition rate reached its maximum value during the 3rd week, and MHCC97-L tumor had a higher inhibition rate of MMSCs than that of MHCC97-H tumor.

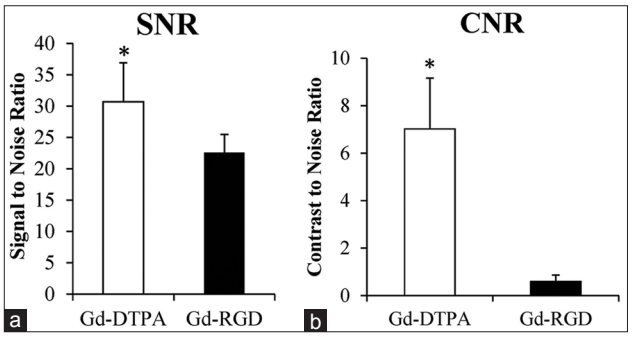

Figure 5: Comparative histograms of SNR and CNR in imaging through two tracers in MHCC97-H model. (a) SNR histogram. (b) CNR histogram. *$P < 0.05$. SNR: Signal-to-noise ratio; CNR: Contrast-to-noise ratio; MHCC97-H: High-metastatic-potential hepatocellular carcinoma.

Polymerase chain reaction results

Tables 3 and 4 compare the expression levels of metastasis-associated genes, OPN, α_v, β_3, and TGFβ1 before and after BMSC intervention.

After the BMSC intervention, the expression levels of OPN, β_3, and TGFβ1 obviously decreased in the MHCC97-H cells ($P < 0.05$), but α_v expression did not significantly change ($P > 0.05$). Co-culturing of MHCC97-L with BMSC significantly decreased the expression levels of OPN, β_3, TGFβ1, and α_v ($P < 0.05$). Thus, metastasis-associated gene expressions in MHCC97-H cells were higher than that in MHCC97-L before and after BMSC intervention.

Discussion

Human bone marrow stem cells mainly include two major types, namely, hematopoietic and mesenchymal stem cells,

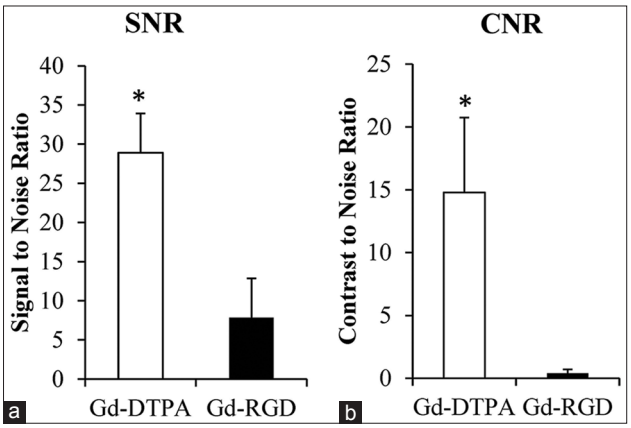

Figure 6: Comparative histograms of SNR and CNR in imaging through two tracers in MHCC97-H model under BMSC intervention. (a) SNR histogram. (b) CNR histogram. *$P < 0.05$. SNR: Signal-to-noise ratio; CNR: Contrast-to-noise ratio; MHCC97-H: High-metastatic-potential hepatocellular carcinoma; BMSC: Bone marrow-derived mesenchymal stem cell.

Table 2: Comparison of SNR and CNR in Gd-RGD imaging before and after BMSC intervention of high- and low-metastatic-potential HCC tissues

Items	MHCC97-H	MHCC97-L	*t*	*P*	BMSC + MHCC97-H	BMSC + MHCC97-L	*t*	*P*
SNR								
Gd-RGD	22.60 ± 2.87	20.63 ± 7.64	1.157	>0.05	7.85 ± 3.24	21.59 ± 7.91	5.126	<0.05
Gd-DTPA	30.71 ± 6.21	39.81 ± 9.21	1.361	<0.05	28.91 ± 10.24	45.40 ± 12.38	4.938	<0.05
CNR								
Gd-RGD	5.32 ± 2.14	21.59 ± 3.24	5.491	<0.05	0.40 ± 0.31	3.94 ± 1.89	4.322	<0.05
Gd-DTPA	7.02 ± 2.14	14.78 ± 5.97	4.307	<0.05	14.78 ± 5.97	18.33 ± 9.41	2.491	<0.05

SNR: Signal-to-noise ratio; CNR: Contrast-to-noise ratio; BMSC: Bone marrow-derived mesenchymal stem cell; RGD: Arginine-glycine-aspartic acid; MHCC97-H: High-metastatic-potential hepatocellular carcinoma; MHCC97-L: Low-metastatic-potential hepatocellular carcinoma; HCC: Hepatocellular carcinoma.

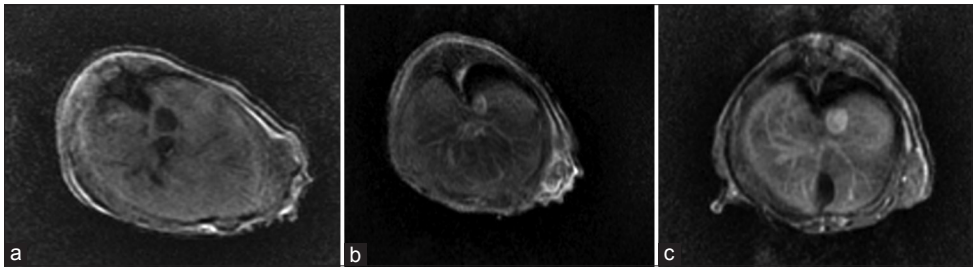

Figure 7: MRI of MHCC97-L tumor-bearing nude mice. (a) MRI scanning TI-weight image. MHCC97-H tumor tissues were located at the mouse armpits. (b) Gd-DTPA-enhanced image. Enhanced pattern of the tumor tissue is similar to that of liver tissue. (c) Gd-RGD-enhanced image. Enhanced pattern of the tumor tissue is lower than that of liver tissue. MRI: Magnetic resonance imaging; MHCC97-L: Low-metastatic-potential hepatocellular carcinoma; MHCC97-H: High-metastatic-potential hepatocellular carcinoma.

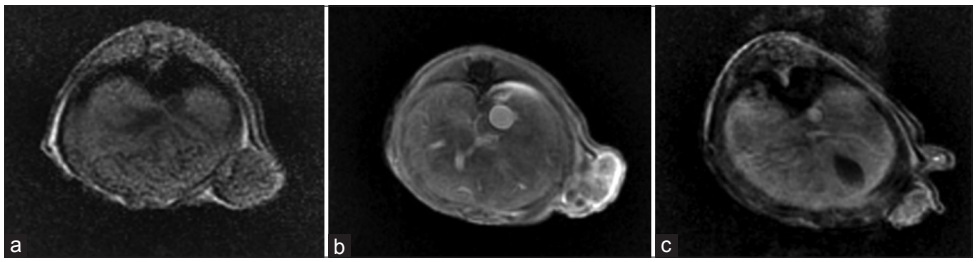

Figure 8: MRI of MHCC97-L tumor-bearing nude mice after BMSC intervention. (a) MRI scanning TI-weighted image. MHCC97-H tumor tissues were located at the mouse armpits. (b) Gd-DTPA-enhanced image. Enhanced pattern of tumor tissue is similar to that of liver tissue. (c) Gd-RGD-enhanced image. Enhanced pattern of tumor tissue enhanced pattern is lower than that of liver tissue. MRI: Magnetic resonance imaging; MHCC97-H: High-metastatic-potential hepatocellular carcinoma; BMSC: Bone marrow-derived mesenchymal stem cell.

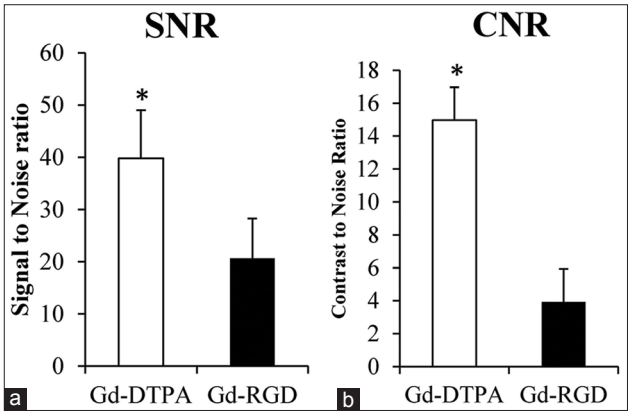

Figure 9: Comparative histograms of SNR and CNR in imaging through two tracers in MHCC97-L HCC model. (a) SNR histogram. (b) CNR histogram. *$P < 0.05$. SNR: Signal-to-noise ratio; CNR: Contrast-to-noise ratio; MHCC97-L: Low-metastatic-potential hepatocellular carcinoma; HCC: Hepatocellular carcinoma.

and the relationship of BMSCs with tumor has become a focus of research. In 1999, Petersen *et al*.[13] verified that oval mouse hepatic cells and hepatocytes can be obtained through bone marrow cell differentiation. Sato *et al*.[14] divided human bone marrow cells into BMSCs, CD34 cells, and non-BMSC/CD34-cells, and found BMSCs as the main source of hepatocytes in the HCC necrotic region. After transplanting bone marrow cells into allyl ethanol, they also found that BMSCs are mainly involved in the cellular expression of hepatic-specific markers in the absence of cellular fusion, causing mouse liver injury. *In vitro* and *in vivo* experiments showed that BMSCs can be distinguished into hepatocytes or hepatocyte-like cells.[15,16] The effects of BMSCs on tumor growth are divided into the tumor growth suppression, such as in lung carcinoma and HCC; tumor growth facilitation, such as in multiple myeloma and breast carcinoma; and no effect on tumor growth, such as in colorectal carcinoma. The BMSC passages adopted in the experiment were within 10 passages with favorable cell growth, and through identification of surface antigen and induced differentiation experiment, conforming to international standards on BMSCs.[17] HCC cell line with high and low metastatic potential is an independent intellectual property right in our country. The cell line was constructed by the Liver Cancer Research Institute of Fudan University. The metastatic behavior of HCC is a key factor that influences prognosis. Thus, observing the influence of BMSC on HCC tissues with high and low metastatic potentials by molecular imaging was the key content in this experimental research.

Target imaging can be achieved through the establishment of a molecular probe as a key part in molecular imaging. Integrin, which is an allotropic cell adhesion molecule, mediates the interaction between cells and ECM, thereby facilitating tumor metastasis. Integrin is a dimer formed from α and β subunits, and the integrin receptor $\alpha_v\beta_3$ is highly abundant on the cell surfaces of multiple tumors and highly expressed in the neovascular endothelial cytomembranes of tumor tissues, despite its absence in mature vascular endothelial cells and most normal organ system receptors.[18] By identifying the specific binding of the RGD sequence together with the ECM protein receptor, the integrin receptor mediates the adhesion and migration of tumor cells. It also mediates tumor growth,

Table 3: Comparison of OPN, αv, β3, and TGFβ1 gene expression before and after MHCC97-H cells were intervened by BMSCs (mean ± SD, ΔΔCt value)

Items	MHCC97-H + BMSCs	MHCC97-H	*t*	*P*
OPN	17.62 ± 0.34	18.69 ± 1.04	1.768	<0.05
β_3	22.09 ± 1.37	24.11 ± 1.26	1.893	<0.05
α_v	20.81 ± 0.21	20.52 ± 0.27	0.691	>0.05
TGFβ1	24.24 ± 0.68	22.65 ± 0.73	2.197	<0.05

OPN: Osteopontin; TGFβ1: Transforming growth factor β-1; MHCC97-H: High-metastatic-potential hepatocellular carcinoma; BMSCs: Bone marrow-derived mesenchymal stem cells.

Table 4: Comparison of OPN, αv, β3, and TGFβ1 gene expression before and after MHCC97-L cells were intervened by BMSCs (mean ± SD, ΔΔCt value)

Items	MHCC97-H + BMSCs	MHCC97-H	*t*	*P*
OPN	13.65 ± 0.78	17.34 ± 1.21	2.568	<0.05
β_3	18.84 ± 1.47	20.14 ± 0.56	1.982	<0.05
α_v	14.56 ± 2.13	19.15 ± 1.98	3.135	<0.05
TGFβ1	18.63 ± 0.95	15.21 ± 1.35	2.849	<0.05

OPN: Osteopontin; TGFβ1: Transforming growth factor β-1; BMSCs: Bone marrow-derived mesenchymal stem cells; MHCC97-H: High-metastatic-potential hepatocellular carcinoma.

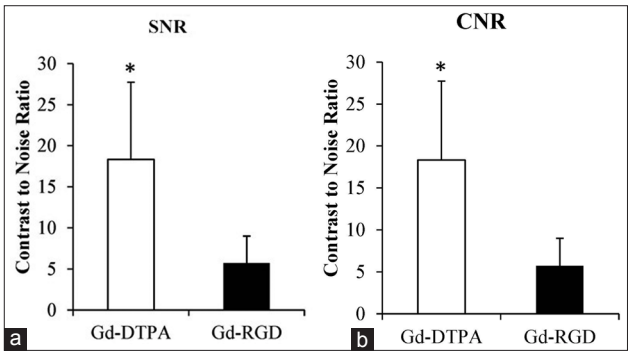

Figure 10: Comparative histograms of SNR and CNR in imaging through two tracers in MHCC97-L HCC model under BMSC intervention. (a) SNR histogram. (b) CNR histogram. *$P < 0.05$. SNR: Signal-to-noise ratio; CNR: Contrast-to-noise ratio; MHCC97-L: Low-metastatic-potential hepatocellular carcinoma; HCC: Hepatocellular carcinoma; BMSC: Bone marrow-derived mesenchymal stem cell.

local infiltration, and metastasis. Vascularization can be evaluated through the development of tumor integrin receptor, RGD.[19] In this study, MRI was carried out by establishing a novel type of molecular imaging probe, Gd-RGD. Given its noninvasive and nonradiation features, MRI has extremely high soft-tissue resolution and spatial resolution and has advantages in the molecular imaging aspect of hepatic diseases. The HCC tissue imaging features of HCCs with high and low metastatic potentials under BMSC intervention were observed. We focused on determining whether Gd-RGD can differentiate HCC tissues with high and low metastatic potentials and whether the tracer can display the changes in tumor metastatic behaviors of HCC tissues under BSMC intervention to provide a basis for carrying out *in vivo* real-time imaging of tumor biological behaviors.

The MRI molecular probe in this research, cRGD-PEG-DGL, was constructed through a coupling reaction, and MRI requirements were met through substantial analysis of Gd^+ required by MRI in the compound. MHCC97-H and MHCC97-L animal models were constructed and placed under BMSC intervention from the 2nd week to the 6th weeks. MR-RGD imaging was implemented, along with Gd-DTPA as a molecular imaging probe control. The imaging results of the two molecular probes showed that, for MHCC97-H and MHCC97-L, MR-RGD was less enhanced than MR-DTPA both before and after BMSC intervention. The reason might be that Gd-DTPA belonged to an extracellular space contrast agent, and it was associated with the richness of the tumor blood supply, whereas Gd-RGD belonged to the tumor-targeted contrast agent and was associated with integrin $\alpha_V\beta_3$ expression in tumor tissues. Moreover, blood supply in tumor tissues was greater than the expression of integrin receptor $\alpha_V\beta_3$ in the tumor tissues. Similarly, semi-quantitative analysis results showed that SNR and CNR of MR-RGD imaging were significantly lower than those of MR-DTPA, indicating that MR-RGD was less enhanced than MR-DTPA.

MR-RGD imaging SNR indicators cannot distinguish between two high and low metastatic potentials in liver cancer with respect to their abilities to differentiate MHCC97-H from MHCC97-L. However, CNR can be used to distinguish MHCC97-H and MHCC97-L, and the CNR of the MHCC97-L tissues was obviously higher than that of MHCC97-H. Therefore, CNR can serve as an index of MR-RGD probe in distinguishing high and low transfer potential. Furthermore, the difference between the two semi-quantitative MR indexes might be associated with the removal of tissue background interference during CNR index calculation, which was superior to SNR calculation.[20] In the detection results of the metastasis-associated indexes such as OPN, α_v, and β_3, only β_3 showed difference between HCCs with high metastatic potential and those with low metastatic potential, indicating that β_3 in the two integrin subunits were the key factors contributing to the difference between the two kinds of HCCs under different metastatic potentials. OPN contained an RGD sequence, which specifically bound to the integrin receptor $\alpha_V\beta_3$ on the cell surface; these sequences facilitate the expression of membrane-type CD44v6 in hepatoma cell lines by binding to its receptor integrin $\alpha_v\beta_3$, and CD44v6 boosts HCC metastasis by binding hyaluronic acid.[21,22]

In contrast to the results before BMSC intervention, both SNR and CNR indexes after BMSC intervention can be used to differentiate HCC tissues with high metastatic potential from those with low metastatic potential. The level of difference in SNR and CNR indexes before and after BMSC intervention under Gd-RGD imaging was obviously higher than those under Gd-DTPA imaging, and the SNR and CNR of the MHCC97-L tissues were obviously higher than those of MHCC97-H tissues. Therefore, Gd-RGD imaging is suitable for differentiating between MHCC97-H and MHCC97-L after BMSC intervention. The expression of

integrin $\alpha_v\beta_3$ in HCC cells after BMSC intervention changed, and PCR analysis of metastasis-associated indexes indicated that expressions of metastasis-associated indexes such as OPN, α_v, and β_3 in HCC cells after BMSC intervention slightly decreased in both MHCC97-H and MHCC97-L tissues. This difference allows Gd-RGD to distinguish MHCC97-H and MHCC97-L after BMSC intervention.

Establishment of MRI through an RGD molecular probe was already studied and reported. Given that Gd^+ is only detectable at the millimole level, a scholar[23] bound the RGD of an integrin $\alpha_V\beta_3$ target with superparamagnetic iron oxide (SPIO) nanoparticles to establish a new type of molecular imaging probe (RGD-SPIO). They found that T2*-weighted MRI can noninvasively identify tumor vessel distribution with different expression levels of integrin $\alpha_V\beta_3$. Another study[24] established a double-mode probe based on ferric oxide nanoparticles, such as RGD-CLIO-Cy5.5. This probe combined the advantages of MRI and fluorescence imaging (high resolution and high sensitivity, respectively). The targeted integrin $\alpha_V\beta_3$ molecular probe was developed and used in clinical research, potentially providing more experimental basis for the definite effect of integrin $\alpha_V\beta_3$ in angiogenic and tumorigenic development. The development may also provide theoretical foundations for the interaction between integrin $\alpha_V\beta_3$ expression, and other neovascularization-associated potential drug targets.

This study is the foundational research before clinical application of stem cell technology, which can provide scientific basis for biological treatment based on BMSC transplantation. The clinical significance of this study is to be able to use multimodality molecular imaging techniques to observe the changes of biological behavior of tumor in body and real time and provide basis for clinical intervention.

The experimental results of tumor tissue weight change in HCC tissues before and after BMSC intervention in this research indicated that tumor weight change rate of high metastatic potential HCC was higher than that of low metastatic potential HCC, certifying that high metastatic potential HCC tissues were more sensitive to BMSC intervention. Differences were observed among the expression levels of tumor proliferation-associated factor TGFβ1 before and after BMSC intervention of HCCs with high and low metastatic potential, and this result agreed with the changes in the weights of the HCCs after the intervention.

In conclusion, the CNR indexes of the Gd-RGD tracers in MRI can be used for differentiating HCC tissues with high metastatic potential from those with low metastatic potential, and the SNR and CNR indexes of the Gd-RGD tracers in MRI after BMSC intervention are useful for distinguishing high- and low-metastatic-potential HCC tissues. Therefore, Gd-RGD imaging is suitable for differentiating the changes between high and low metastatic potentials in HCC tissues after BMSC intervention.

Financial support and sponsorship

This research was supported by grants from the National Natural Science Foundation (No. 81271607), and the National Postdoctoral Science Foundation of China (Grant No. 2015M572810).

Conflicts of interest

There are no conflicts of interest.

References

1. Niess H, Bao Q, Conrad C, Zischek C, Notohamiprodjo M, Schwab F, *et al.* Selective targeting of genetically engineered mesenchymal stem cells to tumor stroma microenvironments using tissue-specific suicide gene expression suppresses growth of hepatocellular carcinoma. Ann Surg 2011;254:767-74. doi: 10.1097/SLA.0b013e3182368c4f.
2. Liu C, Liu Y, Xu XX, Guo X, Sun GW, Ma XJ. Mesenchymal stem cells enhance the metastasis of 3D-cultured hepatocellular carcinoma cells. BMC Cancer 2016;16:1-9. doi: 10.1186/s12885-016-2595-4.
3. Li T, Zhao S, Song B, Wei Z, Lu G, Zhou J, *et al*. Effects of transforming growth factor β-1infected human bone marrow mesenchymal stem cells on high-and low-metastatic potential hepatocellular carcinoma. Eur J Med Res 2015;20:1-11. doi: 10.1186/s40001-015-0144-2.
4. Li T, Song B, Du X, Wei Z, Huo T. Effect of bone-marrow-derived mesenchymal stem cells on high-potential hepatocellular carcinoma in mouse models: An intervention study. Eur J Med Res 2013;18:34. doi: 10.1186/2047-783X-18-34.
5. Li Y, Tang ZY, Ye SL, Liu YK, Chen J, Xue Q, *et al.* Establishment of cell clones with different metastatic potential from the metastatic hepatocellular carcinoma cell line MHCC97. World J Gastroenterol 2001;7:630-6. doi: 10.3748/wjg.v7.i5.630.
6. Li GC, Ye QH, Dong QZ, Ren N, Jia HL, Qin LX. TGF beta1 and related-Smads contribute to pulmonary metastasis of hepatocellular carcinoma in mice model. J Exp Clin Cancer Res 2012;31:93. doi: 10.1186/1756-9966-31-93.
7. Leng L, Wang Y, He N, Wang D, Zhao Q, Feng G, *et al.* Molecular imaging for assessment of mesenchymal stem cells mediated breast cancer therapy. Biomaterials 2014;35:5162-70. doi: 10.1016/j.biomaterials.2014.03.014.
8. Supokawej A, Nimsanor N, Sanvoranart T, Kaewsaneha C, Hongeng S, Tangboriboonrat P, *et al*. Mesenchymal stem cell *in vitro* labeling by hybrid fluorescent magnetic polymeric particles for application in cell tracking. Med Mol Morphol 2015;48:204-21. doi: 10.1007/s00795-015-0102-7.
9. Haris M, Yadav SK, Rizwan A, Singh A, Wang E, Hariharan H, *et al.* Molecular magnetic resonance imaging in cancer. J Transl Med 2015;13:313. doi: 10.1186/s12967-015-0659-x.
10. Weber MR, Zuka M, Lorger M, Tschan M, Torbett BE, Zijlstra A, *et al.* Activated tumor cell integrin αvß3 cooperates with platelets to promote extravasation and metastasis from the blood stream. Thromb Res 2016;140 Suppl 1:S27-36. doi: 10.1016/S0049-3848(16)30095-0.
11. Chen L, Liu Y, Wang W, Liu K. Effect of integrin receptor-targeted liposomal paclitaxel for hepatocellular carcinoma targeting and therapy. Oncol Lett 2015;10:77-84. doi: 10.3892/ol.2015.3242.
12. Zhang C, Yang M, Wang R. The structure-activity relationship of RGD peptides binding to αβ3 integrin and radiolabeled ligand design. J Oncol 2009;15:76-81.
13. Petersen BE, Bowen WC, Patrene KD, Mars WM, Sullivan AK, Murase N, *et al.* Bone marrow as a potential source of hepatic oval cells. Science 1999;284:1168-70. doi: 10.1126/science.284.5417.1168.
14. Sato Y, Araki H, Kato J, Nakamura K, Kawano Y, Kobune M, *et al.* Human mesenchymal stem cells xenografted directly to rat liver are differentiated into human hepatocytes without fusion. Blood 2005;106:756-63. doi: 10.1182/blood-2005-02-0572.
15. Choi D, Kim JH, Lim M, Song KW, Paik SS, Kim SJ, *et al.* Hepatocyte-like cells from human mesenchymal stem cells engrafted in regenerating rat liver tracked with *in vivo* magnetic resonance

imaging. Tissue Eng Part C Methods 2008;14:15-23. doi: 10.1089/tec.2007.0329.
16. Snykers S, Vanhaecke T, Papeleu P, Luttun A, Jiang Y, Vander Heyden Y, *et al.* Sequential exposure to cytokines reflecting embryogenesis: The key for *in vitro* differentiation of adult bone marrow stem cells into functional hepatocyte-like cells. Toxicol Sci 2006;94:330-41. doi: 10.1093/toxsci/kfl058.
17. Dominici M, Le Blanc K, Mueller I, Slaper-Cortenbach I, Marini F, Krause D, *et al.* Minimal criteria for defining multipotent mesenchymal stromal cells. The International Society for Cellular Therapy position statement. Cytotherapy 2006;8:315-7. doi: 10.1080/14653240600855905.
18. Liu G, Fan X, Tang M, Chen R, Wang H, Jia R, *et al.* Osteopontin induces autophagy to promote chemo-resistance in human hepatocellular carcinoma cells. Cancer Lett 2016;383:171-82. doi: 10.1016/j.canlet.2016.09.033.
19. Chen WT, Shih TT, Chen RC, Tu SY, Hsieh WY, Yang PC. Integrin αvß3-targeted dynamic contrast-enhanced magnetic resonance imaging using a gadolinium-loaded polyethylene gycol-dendrimer-cyclic RGD conjugate to evaluate tumor angiogenesis and to assess early antiangiogenic treatment response in a mouse xenograft tumor model. Mol Imaging 2012;11:286-300.
20. Durand DJ, Carrino JA, Fayad LM, Huisman TA, El-Sharkawy AM, Edelstein WA. MRI psychophysics: An experimental framework relating image quality to diagnostic performance metrics. J Magn Reson Imaging 2013;37:1402-8. doi: 10.1002/jmri.23922.
21. Zhang L, Li HY, Yin XL, Xu YP, Chen Y, Xie XY, *et al.* Relative analysis of OPN and its related signal molecules in hepatocellular carcinoma. Chin J Hepatol 2011;19:48-51. doi: 10.3760/cma.j.issn.1007-3418.2011.01.013.
22. Zhang R, Pan X, Huang Z, Weber GF, Zhang G. Osteopontin enhances the expression and activity of MMP-2 via the SDF-1/CXCR4 axis in hepatocellular carcinoma cell lines. PLoS One 2011;6:1-8. doi: 10.1371/journal.pone.0023831.
23. Liu C, Liu DB, Long GX, Wang JF, Mei Q, Hu GY, *et al*. Specific targeting of angiogenesis in lung cancer with RGD-conjugated ultrasmall superparamagnetic iron oxide particles using a 4.7T magnetic resonance scanner. Chin Med J 2013;126:2242-7.
24. Jarzyna PA, Deddens LH, Kann BH, Ramachandran S, Calcagno C, Chen W, *et al*. Tumor angiogenesis phenotyping by nanoparticle-facilitated magnetic resonance and near-infrared fluorescence molecular imaging. Neoplasia 2012;14:964-73.